surfaces

Article

DFT and MCDS Outcome for a Comparative Analysis of NO, NO_2, SO, SO_2 and SO_3 Gas Adsorption onto a $NaMgPO_4$ (033) Surface

Jamal Attarki [1], Malika Khnifira [1], Wafaa Boumya [1], Hind Hajjaoui [1], Anass Mahsoune [1], M'hamed Sadiq [1], Mounia Achak [2,3], Noureddine Barka [1,*] and Mohamed Abdennouri [1]

[1] Multidisciplinary Research and Innovation Laboratory, FP Khouribga, Sultan Moulay Slimane University of Beni Mellal, BP. 145, Khouribga 2500, Morocco; jamalattarkki@gmail.com (J.A.); m.khnifira@uhp.ac.ma (M.K.); wafboumya@gmail.com (W.B.); hind.hajjaoui@usms.ac.ma (H.H.); anassmahsoune@gmail.com (A.M.); sadiqmhamed@hotmail.com (M.S.); m.abdennouri@usms.ma (M.A.)

[2] Laboratoire des Sciences de l'Ingénieur pour l'Energie, Ecole Nationale des Sciences Appliquées, Chouaib Doukkali University, El Jadida 24000, Morocco; achak_mounia@yahoo.fr

[3] Chemical & Biochemical Sciences, Green Process Engineering, CBS, Mohammed VI Polytechnic University, Ben Guerir 43150, Morocco

* Correspondence: barkanoureddine@yahoo.fr; Fax: +212-523-49-03-54

Abstract: The research purpose of this work is to examine the adsorption interaction of gaseous molecules (GMs), such as NO, NO_2, SO, SO_2, and SO_3, with the surface of sodium magnesium phosphate $NaMgPO_4$ (033), in a neutral medium, using two different computational methods: density functional theory (DFT) and Monte Carlo dynamic simulation (MCDS). Various quantum and dynamic descriptors, such as global and local quantum descriptors and the radial distribution function (RDF), are also evaluated and discussed. The data obtained revealed that the NO_2 molecule has a small energy gap (0.363 eV) when compared to the other molecules, which means that it is highly reactive and is liable to adsorb, or stick, to the surface of $NaMgPO_4$ (033). Furthermore, this NO_2 molecule exhibits good adsorption in aqueous media, returning to the lowest global hardness value (0.1815 eV). MCDS predicted adsorption energies of −874.03, −819.94, −924.81, −876.33, and −977.71 kcal/mol for NO, NO_2, SO, SO_2, and SO_3, respectively. These energies are negative, implying that adsorption occurs spontaneously. Thus, the side views indicated which SO, NO, and SO_3 molecules are adsorbed in parallel to $NaMgPO_4$ and the other SO_2 and NO_2 molecules are adsorbed horizontally. Eventually, the theoretical results reveal that the studied gaseous molecules interact strongly with $NaMgPO_4$. The result obtained by radial distribution function (RDF) analysis for all complexes below 3.5 Å confirm that the adsorption is of the chemi1cal type.

Keywords: gas adsorption; sodium magnesium phosphate; DFT; Monte Carlo simulation

check for updates

Citation: Attarki, J.; Khnifira, M.; Boumya, W.; Hajjaoui, H.; Mahsoune, A.; Sadiq, M.; Achak, M.; Barka, N.; Abdennouri, M. DFT and MCDS Outcome for a Comparative Analysis of NO, NO_2, SO, SO_2 and SO_3 Gas Adsorption onto a $NaMgPO_4$ (033) Surface. *Surfaces* **2023**, *6*, 450–465. https://doi.org/10.3390/surfaces6040030

Academic Editors: Gaetano Granozzi and Michalis Konsolakis

Received: 6 September 2023
Revised: 1 November 2023
Accepted: 7 November 2023
Published: 13 November 2023

1. Introduction

Due to global climate change or air pollution, there is an immediate need to reduce exhaust gases [1]. The substantial emission of harmful gases, such as NO_x, SO_x, and CO_x, from the automotive industry is released into the atmosphere, leading to various health problems, including infectious diseases and respiratory conditions [2–4]. Acid rain, photochemical smog, and ozone depletion are just a few of the environmental issues that also promote the corrosion or rust of equipment and industrial instruments caused by the nitrogen oxides NO_x and sulfur oxides SO_x released by cars and coal-fired power plants [5]. Therefore, the elimination of NO_x and SO_x is imperative. The regular measurement of gas concentration is necessary to avoid the hazards of these gases. Notably, advancements in NO_x removal technology have received significant attention, resulting in a relatively rapid reduction in NO_x air pollution. Technologies such as NO oxidation have become increasingly important in NO_x removal methods, like NO_x storage and reduction [6,7], dry sorbent injection [8], absorption in wet flue gas desulfurization [9,10], and the use of catalysts, considered a common method for removing these harmful gases from automotive emissions [11–13]. Unfortunately, meeting international regulations for NO_x removal by the three-way catalyst in a diesel engine under operating conditions is challenging due to the abundance of oxygen in the emissions [14,15]. Considering that sulfur monoxide, dioxide, and trioxide (SO_x) release disagreeable and offensive odors into the atmosphere, several studies have focused on SO_x adsorption onto various surfaces [16–20]. However, the advanced technologies for the elimination of gaseous molecules entail a high energy cost. Improving the efficiency and reducing the cost of the elimination of these studied molecules entails integrating simple and efficient removal processes, like adsorption and membrane separation technologies. The adsorption process is the most efficient because of its lower environmental impact and lower cost [21–24]. Furthermore, research has revealed that phosphate adsorbents have a significant adsorption capacity for both organic and inorganic pollutants due to their natural abundance [25]. Many researchers have focused for the adsorption of various gaseous molecules on different adsorbents. For instance, Sajid et al. focused on the adsorption of gaseous molecules with $Be_{12}O_{12}$, $Mg_{12}O_{12}$, and $Ca_{12}O_{12}$. The results indicated that the adsorption energies of $N_2O@Ca_{12}O_{12}$, $NO_2@Ca_{12}O_{12}$, $NO@Ca_{12}O_{12}$, $H_2S@Ca_{12}O_{12}$, $SO_2@Ca_{12}O_{12}$, and $SO_3@Ca_{12}O_{12}$ were −11. 79, −46.53, −26.51, −50.26, −78.64, and −123.62 kcal/mol, respectively [26]. Similarly, Gao et al. studied the adsorption of NO, NO_2, SO_2, and SO_3 on single vacancy graphene with three doped nitrogen atoms (Ni-SVN3/GN) on graphene adsorbent. According to their findings, the adsorption energy values for NO, NO_2, SO_2, and SO_3 were 3.51 eV, 2.50 eV, 1.72 eV, and 2.37 eV, respectively [27]. Furthermore, organic aza-macrocyclic hexaazabipyH2 (HA) was utilized as an adsorbent to remove gaseous molecules, such as N_2O, NO_2, H_2S, SO_2, and SO_3. The obtained data revealed the interaction energies to be −4.80, −4.86, −7.09, −7.42, and −11.64 kcal/mol for NO_2, N_2O, H_2S, SO_2, and SO_3, respectively [28]. Subsequently, we conducted a theoretical study of NO, NO_2, SO, SO_2, and SO_3 gases on a $NaMgPO_4$ surface. $NaMgPO_4$ is a member of the $ABPO_4$ family with A denoting alkaline metals (A = Li, Na, and K) and B denoting alkaline earth metals (M = Mg, Ca, Sr, and Ba), which is gaining popularity. $NaMgPO_4$ is especially intriguing due to its luminescent properties, remarkable structural properties, and better chemical and thermal stability [29].

In this context, the focus of the study is to use DFT and MCDS to examine the mechanism of interaction behavior of NO, NO_2, SO, SO_2, and SO_3 molecules on the surface of $NaMgPO_4$ (033) in aqueous media. The adsorption of the studied molecules onto the surface has significant applications in many industrials processes. Our results show that SO, NO, SO_2, NO_2, and SO_3 molecules are adsorbed in parallel/horizontally on the $NaMgPO_4$ surface. GM adsorption on the $NaMgPO_4$ (033) face is chemical in nature, indicating a strong interaction.

2. Materials and Methods

2.1. Quantum Chemical Calculations

In this study, the Gaussian 09 package was implemented to conduct full DFT calculations. The molecule's geometry was optimized using the B3LYP functional, which is commonly used in these calculations because it provides a good balance of accuracy and computational efficiency [30]. Additionally, the LanL2DZ basis was applied in the calculations [31]. It was selected as the most precise basis set from the available options. The computation was conducted with the minimum energy and with water as the solvent. This calculation is typically used to investigate a variety of characteristics, including the electronic properties of gaseous molecules, the impact of the energies of the lowest and highest occupied molecular orbitals (LUMOs and HOMOs), and the distinction between both of them. As a result, the DFT approach has grown in popularity in recently [32]. Quantum reactivity descriptors are a set of molecular properties that are calculated from the output of quantum chemical calculations and are used to assess the chemical reactivity of a molecule. The most important molecular descriptors extracted directly from the output files are those related to molecule reactivity, which include the energy of the lowest unoccupied molecular orbital (E_{LUMO}), the energy of the highest occupied molecular orbital (E_{HOMO}), electronic affinity (AE = $-E_{LUMO}$), ionization potential (IE = $-E_{HOMO}$), energy gap (Eg = $E_{LUMO} - E_{HOMO}$), hardness (η), absolute electronegativity (χ), global softness (S), global electrophilicity index (ω), back donation energy ($E_{b\text{–}d}$), the number of transferred electrons (ΔN), and chemical potential (μ). These descriptors are used to understand the preferred adsorption sites of compounds as well as to predict their reactivity and predict the outcomes of chemical reactions. The following mathematical expressions were used to calculate the above parameters [33–36].

$$E_g = E_{LUMO} - E_{HOMO} \tag{1}$$

$$\mu_{CP} = -\chi = -\frac{(IP + EA)}{2} \tag{2}$$

$$\eta = \frac{(IP - EA)}{2} \tag{3}$$

$$\frac{1}{S} = 2\eta = \left(\frac{\partial \mu}{\partial N}\right)_{v(r)} = \left(\frac{\partial^2 E}{\partial^2 N}\right) \tag{4}$$

$$\omega = \frac{\chi^2}{2\eta} = \frac{\mu^2}{2\eta} \tag{5}$$

$$E_{b-d} = -\frac{\eta}{4} \tag{6}$$

$$\Delta N = \frac{\chi}{2\eta} \tag{7}$$

2.2. Monte Carlo Dynamic Simulation Details

To conduct our investigation of the adsorption characteristics of NO, NO_2, SO, SO_2, and SO_3 compounds on the $NaMgPO_4$ (033) surface, MCD computations were conducted using the Material Studio 8.0 Software (Accelrys; BIOVIA, Dassault Systems, San Diego, CA 92121, USA) [37,38]. In a simulation box (20 Å)^3, the interaction of a single molecule (NO, NO_2, SO, SO_2, or SO_3) with the $NaMgPO_4$ (033) surface was simulated. As shown in Figure 1, a 20 Å thickness vacuum slab was built above the $NaMgPO_4$ (033) face, which was then enlarged into a (4 × 4 × 4) supercell. The (033) plane was used for all molecular systems (M: NO, NO_2, SO, SO_2, and SO_3/500 H_2O/$NaMgPO_4$ (033)). A liquid solution of 500 H_2O molecules was appended to predict the solvent effect, which can influence the adsorption process. This simulation was set to run for a total simulation time of 500 ps at a 1.0 bar of pressure. The universal force field was used to compute the energy values and search for equilibrium configurations during the over-all simulation procedure with the charges for the used current. Atom-based and Ewald & Group summation methods were performed to obtain the potential energy of the complex in the simulation procedure. The fine quality choice was adopted to assure preciseness in the analysis of electrostatic interaction contributions. The purpose of this calculation study was to understand the interaction between GMs and the $NaMgPO_4$ (033) face and to discover the relationship between the reactivity of the molecules and their ability to adsorb onto the surface. By calculating the energy adsorption (E_{ads}) of each of the molecules, it is possible to determine which molecules have a stronger affinity for the surface and to identify any small energy adsorption centers that may be present. Thus, the E_{ads} emitted when the expanded adsorbate constituent is simultaneously deposited on the adsorbent was calculated using the following expression [39].

$$E_{ads} = E_{surface/molecule} - (E_{surface} + E_{molecule}) \tag{8}$$

where $E_{molecule/surface}$ reflects the total energy of the GM and $NaMgPO_4$ (033) face system, $E_{surface}$ represents the total energy of the isolated $NaMgPO_4$ (033), and $E_{Molecule}$ represents the total energy of the isolated GMs.

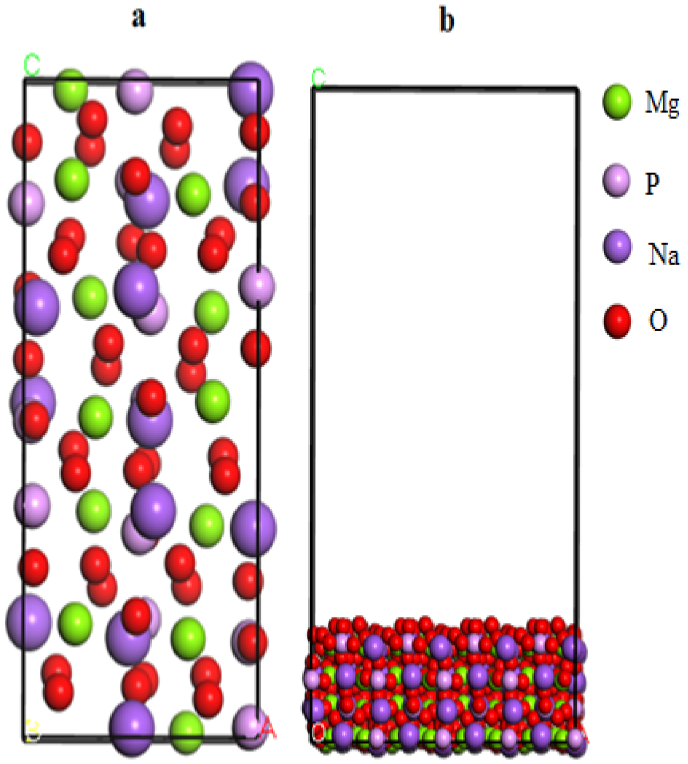

Figure 1. Supercell of $NaMgPO_4$ (**a**) and $NaMgPO_4$ (033) surface model (**b**).

The RDF analysis enabled us to comprehend the nature of the interactions between the adsorbent and the adsorbate, such as whether they are physisorbed (held by weak van der Waals forces) or chemisorbed (held by chemical bonds) [40,41]. It is often used to study the structure and properties of materials, such as adsorbents and adsorbates, in order to understand their behavior during the adsorption process. Thus, RDF or g(r) represents the probability of finding a particle at a distance r from a reference particle within a system, rather than specifically an atom from another atom. In this case, "r" represents the distance between two particles. The g (r) to perform the distance analysis between two atoms, and α and β are determined using the following expression.

$$g_{\alpha\beta}(r) = \frac{1}{\langle \rho_\beta \rangle_{local}} \times \frac{1}{N_\alpha} \left(\sum_{i\in\alpha}^{N_\alpha} \sum_{i\in\beta}^{N_\beta} \frac{\delta(r_{ij} - r)}{4\pi r^2} \right) \tag{9}$$

where $\langle \rho_\beta \rangle$ local represents the particle density of β averaged over all shells around particle α. N_α is the number of particles and r_{ij} is the positions of particles i and j.

3. Results

3.1. Frontier Molecular Orbitals and MEP

By plotting the HOMO (highest occupied molecular orbital) and LUMO (lowest unoccupied molecular orbital) densities and the MEP (molecular electrostatic potential) of the GMs under study in aqueous media, determined by the B3LYP functional with a LanL2DZ basis, as shown in Figure 2, it was possible to gain insights into the reactivity and stability of the GMs [42]. When the HOMO and LUMO densities are concentrated in different regions of the molecule, it means a higher reactivity of the molecules. Similarly, A positive MEP in one region of the molecule and negative in another indicates that the molecule is unstable and prone to reacting with other molecules. As illustrated in Figure 2, in SO_2 and SO_3 molecules, the HOMOs are usually localized on the oxygen atoms. Conversely, the HOMO and LUMO electron densities for the SO, NO, and NO_2 molecules are centered on the entirety of the three molecules. Furthermore, the HOMO electron density provides information about the sites of the molecule that are more likely to donate electrons to an acceptor molecule's appropriate orbital. This can lead to a chemical reaction or change in the electronic properties of the adsorbent. In contrast, the LUMO density is frequently employed to describe the reactivity of GMs, since it is the orbital that is the most available to accept an electron from the $NaMgPO_4$ (033) face. Thus, Figure 2 indicates that the LUMO is located mostly on the O, S, and N atoms of the investigated molecules, except for the SO_3 molecule, where it is present on the oxygen atom. This suggests that these atoms are the most likely sites for electron transfer to occur during the adsorption process [43]. It can also be observed that the adsorption process of GMs on the $NaMgPO_4$ (033) face is likely mediated by the interaction of the nitrogen, oxygen, and sulfur atoms with the surface. These findings were confirmed by MEP, which represents the molecule's electronegativity and electropositivity. As shown in Figure 2, the electrostatic potentials on the MEP map are represented by various hues, with the electrostatic potential value increasing steadily from red to blue. The nucleophilic regions are represented in blue and light blue, while the electrophilic regions are represented in red. Furthermore, the green color represents the neutral charge. The NO, NO_2, SO, SO_2, and SO_3 molecules demonstrate that the N and S atoms have positive electrostatic potentials, ranging between 0.0083 and 0.0323 a.u. for the N atom and varying between 0.0425 and 0.0586 a.u. for the S atom, whereas the oxygen atoms have negative electrostatic potentials raging between −0.0459 and −0.0143 a.u. Most electron-rich areas (electrophilic sites) are mainly found near oxygen atoms, and electron-deficient areas are found near the N atoms and S atoms of the NO, NO_2, SO, SO_2, and SO_3 molecules. This indicates that negatively charged heteroatoms can interact with the adsorbent surface via an electron donor–acceptor reaction [44]. This type of interaction can be important in various chemical reactions and processes, such as adsorption.

3.2. Global Quantum Descriptors

To comprehend the reactivity of the studied molecules, Table 1 lists the calculated parameters disregarding their structural or electronic characteristics in aqueous media. The E_{LUMO} is a critical factor in determining a molecule's ability to accept electrons. In general, a molecule with a low E_{LUMO} is more inclined to accept electrons from the adsorbent surface, while a molecule with a high E_{LUMO} is less inclined to do so. Furthermore, the E_{HOMO} also expresses a compound's capacity to provide electrons. Molecules with a high HOMO energy are more likely to donate electrons to other molecules, making them more reactive. On the other hand, molecules with a low HOMO energy are less inclined to provide electrons and may be less reactive as a result. Nonetheless, the E_{HOMO} can be an important factor when predicting and designing molecules for chemisorption applications. There are, however, other important descriptors for understanding many chemical reactions. Table 1 displays the obtained global parameters for the reactivity of NO, NO_2, SO, SO_2, and SO_3 species.

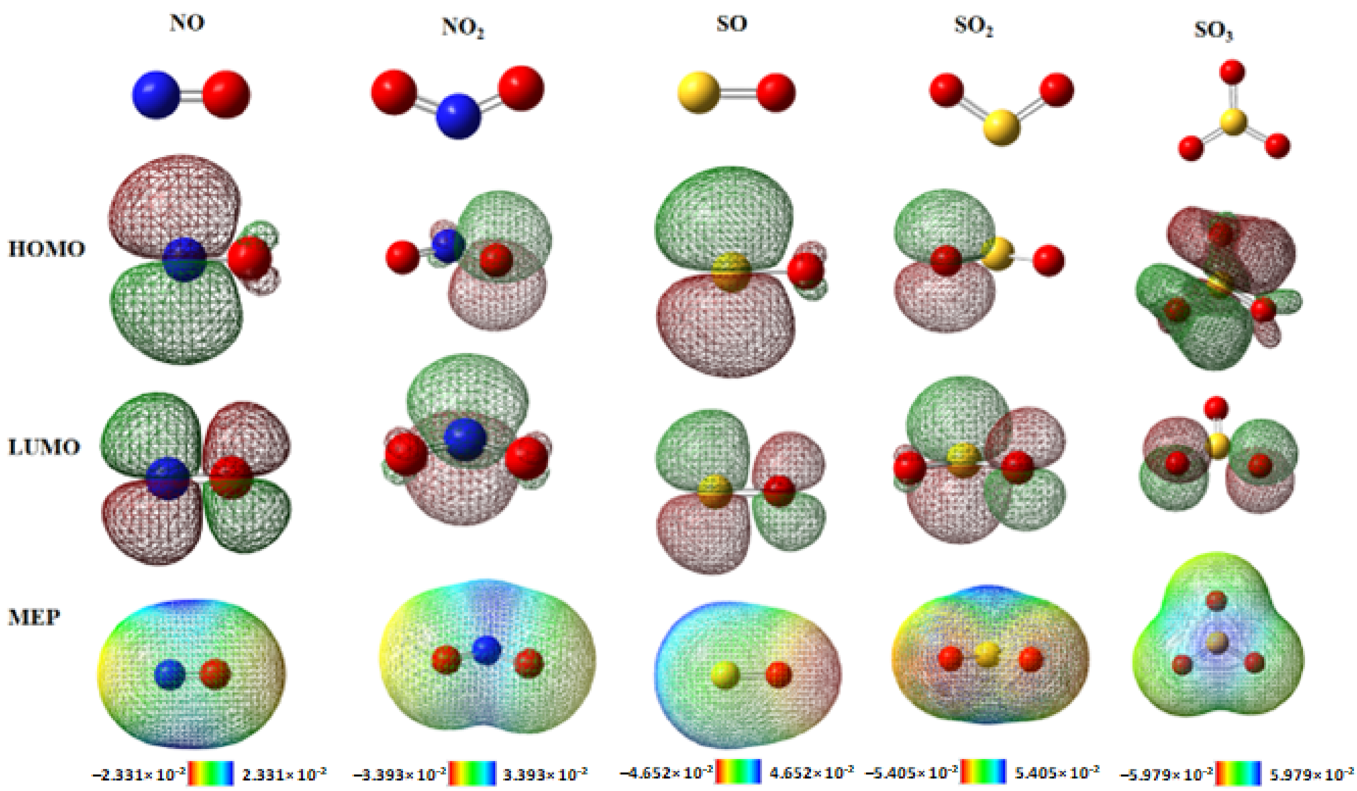

Figure 2. HOMOs, LUMOs, and MEPs for GMs in aqueous media.

Table 1. Quantum chemical parameters (in eV) of the GMs in aqueous media.

	Parameter (eV)									
Molecule	E_{HOMO}	E_{LUMO}	E_g	S	χ	η	μ	ω	E_{b-d}	ΔN
NO	−9.434	−3.236	6.198	0.323	6.335	3.099	−6.335	−1.584	−0.775	1.022
NO_2	−9.766	−9.403	0.363	5.510	9.584	0.181	−9.584	−2.396	−0.045	26.403
SO	−8.123	−5.297	2.825	0.708	6.710	1.412	−6.710	−1.677	−0.353	2.375
SO_2	−9.100	−6.461	2.639	0.758	7.781	1.320	−7.781	−1.945	−0.330	2.948
SO_3	−12.193	−10.318	1.874	1.067	11.255	0.937	−11.255	−2.814	−0.234	6.004

The obtained results show that the variation in E_{LUMO} values is in the following order in the aqueous phase: SO_3 < NO_2 < SO_2 < SO < NO. On the other hand, E_{HOMO} follows the sequence SO_3 < NO_2 < SO_2 < NO < SO. Notably, the SO molecule has a higher E_{HOMO} value than the NO_2, NO, SO_2, and SO_3 molecules, indicating that it is more likely to donate electrons. On the other hand, the SO_3 molecule has a lower E_{LUMO} value than the NO_2, SO, SO_2, and NO molecules, indicating that it is more likely to accept electrons [45]. This means that SO is more likely to act as an electron donor in a chemical reaction, while SO_3 is more likely to act as an electron acceptor. The energy gap (E_g) explains the adsorbate molecule's reactivity (such as a GM) for adsorption on the adsorbent surface (such as $NaMgPO_4$). The lower value of E_g of the NO_2 molecule indicates that it is easier to remove an electron from the adsorbate molecule or to add an electron to it, making it more reactive and more likely to adsorb onto the surface of $NaMgPO_4$ [46]. As shown in Table 1, the quantum chemistry calculations show that the E_g of the NO_2 molecule is the smallest compared to that of the other molecules, which show a decrease in E_g values for the NO, SO, SO_2, SO_3, and NO_2 molecules of 6.1979 > 2.8251 > 2.6395 > 1.8745 > 0.363 eV, respectively. In addition, the species' total number of transported electrons or ΔN was estimated for each species. The outcomes are presented in Table 1. It has been reported that ΔN reveals a molecule's propensity to donate electrons [47,48]. In fact, for a molecule's inclination to donate electrons to electron-deficient species to be high, it is necessary that the value of ΔN is positive and high. In the case of the studied molecules, a higher ΔN was noticed for the NO_2 molecule, which involves a stronger propensity to interact with the $NaMgPO_4$ (033) face (i.e., a higher inclination to adsorb onto the adsorbent surface), suggesting a strong adsorption capacity on the adsorbent surface. The studied molecules' ΔN values were in the following order 26.4033 > 6.0045 > 2.9478 > 2.3751 > 1.0221 eV for NO_2, SO_3, SO_2, SO, and NO respectively. Additionally, back donation energy, or E_{b-d}, is a measure of the energy required for an electron to transfer from a GM to a $NaMgPO_4$ surface. The results show that E_{b-d} is negative for all molecules, suggesting that the molecule investigated has an energetically favorable back donation to the $NaMgPO_4$ surface. Moreover, hardness (η) and softness (S) are two other properties that can be employed to analyze a molecule's stability and reactivity. In general, molecules that are harder are more stable and less reactive, while molecules that are softer are less stable and more reactive. The NO_2 molecule has a low hardness and high softness value, calculated at 0.181 eV and 5.510 eV, respectively, than the other NO, SO, SO_2, and SO_3 molecules, which means they are more reactive and less stable. Furthermore, the results of E_{b-d}, ΔN, S, and η are in agreement. All studied NO, NO_2, SO, SO_2, and SO_3 molecules ha a negative chemical potential calculated at −6.335, −9.584, −6.710, −7.781, and −11.255 eV, respectively. This means that GMs may be able to form strong interactions with other species in the system, resulting in the formation of new chemical bonds. Alternatively, GMs may be capable of stabilizing the system by filling empty sites.

3.3. Mulliken Charge Distribution

The analysis of the Mulliken population typically provides details about a molecule's active sites. The active sites are the nitrogen (N), sulfur (S), and oxygen (O) atoms, which are critical components in the reactivity of the compounds under investigation. The calculated Mulliken charges of these three atoms in the NO, NO_2, SO, SO_2, and SO_3 molecules are listed in Table 2. The outcomes show that the oxygen atoms have a higher negative charge in all investigated molecules, suggesting that these atoms are the likely active sites for attacking the adsorbent atoms. Consequently, these active sites will facilitate the adsorption process of the selected molecules onto the $NaMgPO_4$ surface by increasing the adsorption energy. On the other hand, the nitrogen and sulfur atoms in these molecules have a positive Mulliken population, indicating that they are electron-deficient and may be more likely to accept electrons from other atoms The oxygen Mulliken population values of the studied molecules were as follows: −0.7797, −0.1389, −0.5456, −0.5216, −0.4687, −0.4535, and −0.4531 for NO, NO_2, SO, SO_2, and SO_3, respectively.

Table 2. Mulliken atomic charges obtained for each molecule.

	N	**O**	**S**
NO	0.7797	−0.7797	
NO_2	0.2779	−0.1389	
SO		−0.5456	0.5456
SO_2		−0.5216	1.0432
SO_3		−0.4687 −0.4535 −0.4531	1.3753

As it can be seen from this result, oxygen atoms are capable of conferring electrons to $NaMgPO_4$ atoms to create a coordination bond. This type of bond is often seen in compounds containing transition metals, where the metal atom acts as the central atom and the ligand atoms (such as oxygen) donate their electrons to form the bond.

3.4. Fukui Function Calculations

The Fukui function (f) measures the electron density at a particular site in a molecule. It can be utilized to identify the most reactive sites in a molecule and to predict the reactivity of a molecule towards different types of reagents. The different parts of the molecule can be distinguished based on their chemical characteristics using the condensed Fukui function and local reactivity indices [49]. These indices can be used to predict which parts of a molecule are more likely to react with other molecules, and can be useful for understanding the behavior of a molecule in chemical reactions. The Fukui indices are descriptive terms that identify the kind of attack (radical, electrophile, or nucleophile, or any combination of the three). The possibility of the adsorption of the adsorbate on the adsorbent is recalled by the reactive sites with high negative charge densities. A nucleophile is a species that is attracted to electron-poor regions and tends to attack atoms or functional groups with a high f^+ value. On the other hand, an electrophile is attracted to electron-rich regions and tends to attack atoms or functional groups with a high f^- value. As it is well-known, $\Delta f < 0$ represents a suitable region for the electrophilic attack. Moreover, $\Delta f > 0$ is the most expected region of a nucleophilic attack. The Fukui indices can be calculated by employing the following formulae for three different situations [47]:

For a reaction with nucleophiles:

$$f_i\left(\vec{r}\right)^+ = q_i(N+1) - q_i(N) \tag{10}$$

For a reaction with electrophiles:

$$f_i\left(\vec{r}\right)^- = q_i(N) - q_i(N-1) \tag{11}$$

where q_N, q_{N+1}, and q_{N-1} are the atomic charges of the systems with N, N + 1, and N − 1 electrons, respectively, at a particular point r in the molecule.

An atom's electrophilic and nucleophilic attacks in a molecule are defined as follows:

$$\Delta f_i = f_i\left(\vec{r}\right)^+ - f_i\left(\vec{r}\right)^- \tag{12}$$

The f_k+ and $f_k{}^-$ parameters' absolute values increase with the increase in the tendency of accepting and donating electrons, respectively.

The Fukui indices of the GMs were calculated to predict the center of nucleophilic attack ($f_i{}^+$) and electrophilic attack ($f_i{}^-$), which are depicted in Table 3. NO has the highest $f_i{}^+$ and $f_i{}^-$ values, observed on N_2 with values of 0.584 and 0.637, respectively, which is the most likely nucleophilic and electrophilic attack site. For NO_2, the highest values for $f_i{}^+$ and $f_i{}^-$ are found O1 and O2, with values of 0.33 and 0.348 (nucleophilic and electrophilic attacks), respectively. Also, for SO, the most probable nucleophilic attack ($f_i{}^+$) and electrophilic attack ($f_i{}^-$) are S1, with values of 0.79 and 0.812, respectively. For SO_2, the highest value for $f_i{}^+$ is found on O_2 and O_3, with a value of 0.369 (nucleophilic attack), and the highest value for $f_i{}^-$ is found on S1, with a value of 0.583 (electrophilic attack). Thus, SO_3 has the highest value for $f_k{}^+$ on O_2, with a value of 0.323 (nucleophilic attack center), and $f_i{}^-$ on S1, which represents the most probable electrophilic attack center with a value of 0.558. The higher the absolute value of the Fukui indices $f_i{}^+$ and $f_i{}^-$, the greater the susceptibility to accept and donate electrons. As a result, the studied molecules have the most active sites for the electron donation/acceptance type of interaction, implying an ease of adsorption onto the adsorbent surface.

Table 3. Fukui indices calculated using the B3LYP/LanL2DZ method.

Molecule	Atom	$q_i(N)$	$q_i(N+1)$	$q_i(N-1)$	f_i^+	f_i^-	Δf
NO	O1	−0.202	0.214	−0.565	0.416	0.363	0.053
	N2	0.202	0.786	−0.435	0.584	0.637	−0.053
NO_2	N1	0.498	0.194	0.837	−0.304	−0.339	0.035
	O2	−0.249	0.081	−0.597	0.33	0.348	−0.018
	O3	−0.249	0.081	−0.597	0.33	0.348	−0.018
SO	S1	0.584	1.374	−0.228	0.79	0.812	−0.022
	O2	−0.584	−0.374	−0.772	0.21	0.188	0.022
SO_2	S1	1.423	1.684	0.84	0.261	0.583	−0.322
	O2	−0.711	−0.342	−0.92	0.369	0.209	0.16
	O3	−0.711	−0.342	−0.92	0.369	0.209	0.16
SO_3	S1	1.985	2.025	1.427	0.04	0.558	−0.518
	O2	−0.662	−0.339	−0.809	0.323	0.147	0.176
	O3	−0.662	−0.341	−0.809	0.321	0.147	0.174
	O4	−0.661	−0.345	−0.809	0.316	0.148	0.168

3.5. Monte Carlo Dynamic Simulation Study

The MCDS was utilized to understand and explain the interactions of gaseous molecules with the $NaMgPO_4$ (033) surface in aqueous media. Furthermore, the adsorbent and adsorbate molecules' combined potential and interaction energies were simulated by MCDS in a simulation box ($45\times 45 \times 45$ Å^3) with periodic boundary conditions. Figure 3 depicts the electrostatic, intermolecular, van der Waals, total, and total average energies for the adsorption of gaseous molecules on the adsorbent surface in aqueous media. As shown in Figure 3, the intramolecular energy is positive and stagnant. In fact, the complex $SO_3/NaMgPO_4$ is superior to the other molecules with a value of 530 kcal/mol, meaning that it is likely to be more stable. The order of intramolecular energies for the other complexes suggests that the stability of the complexes decreases as the intramolecular energy decreases. In the same positive stage, the intramolecular energy obtained from the studied complexes has a following order: $SO_3/NaMgPO_4$ > $SO/NaMgPO_4$ > $SO_2/NaMgPO_4$ > $NO_2/NaMgPO_4$ > $NO/NaMgPO_4$ (530, 442, 401, 386, and 375 kcal/mol, respectively). Nevertheless, the electrostatic energy for all studied complexes is zero, which means that the distribution of electric charge within the complexes is balanced and there are no net forces between the atoms. However, the average total energy for each complex is positive, with values for $NO/NaMgPO_4$ ranging from 0 to 176 kcal/mol, for $NO_2/NaMgPO_4$ from 129 to 232 kcal/mol, for $SO/NaMgPO_4$ from 183 to 442 kcal/mol, for $SO_2/NaMgPO_4$ from 125 to 307 kcal/mol, and for $SO_3/NaMgPO_4$ from 237 to 463 kcal/mol.

Then, the chemical complexes $SO/NaMgPO_4$ and $SO_3/NaMgPO_4$ have positive total energy values ranging from 49 to 546 kcal/mol and 144 to 620 kcal/mol, respectively, suggesting that the complexes are reactive and are likely to break apart or react with other molecules under certain conditions. $NO/NaMgPO_4$, $NO_2/NaMgPO_4$, and $SO_2/NaMgPO_4$ have both positive and negative total energy simultaneously, meaning that the complexes can absorb or release energy through various interactions or processes. Lastly, the van der Waals bonds have a negative and positive value for each of the complexes that were studied, with values that are no greater than −448 kcal/mol and 135 kcal/mol, respectively, indicating that the attractive and repulsive forces between the molecules in the complexes are not constant and may change under different conditions.

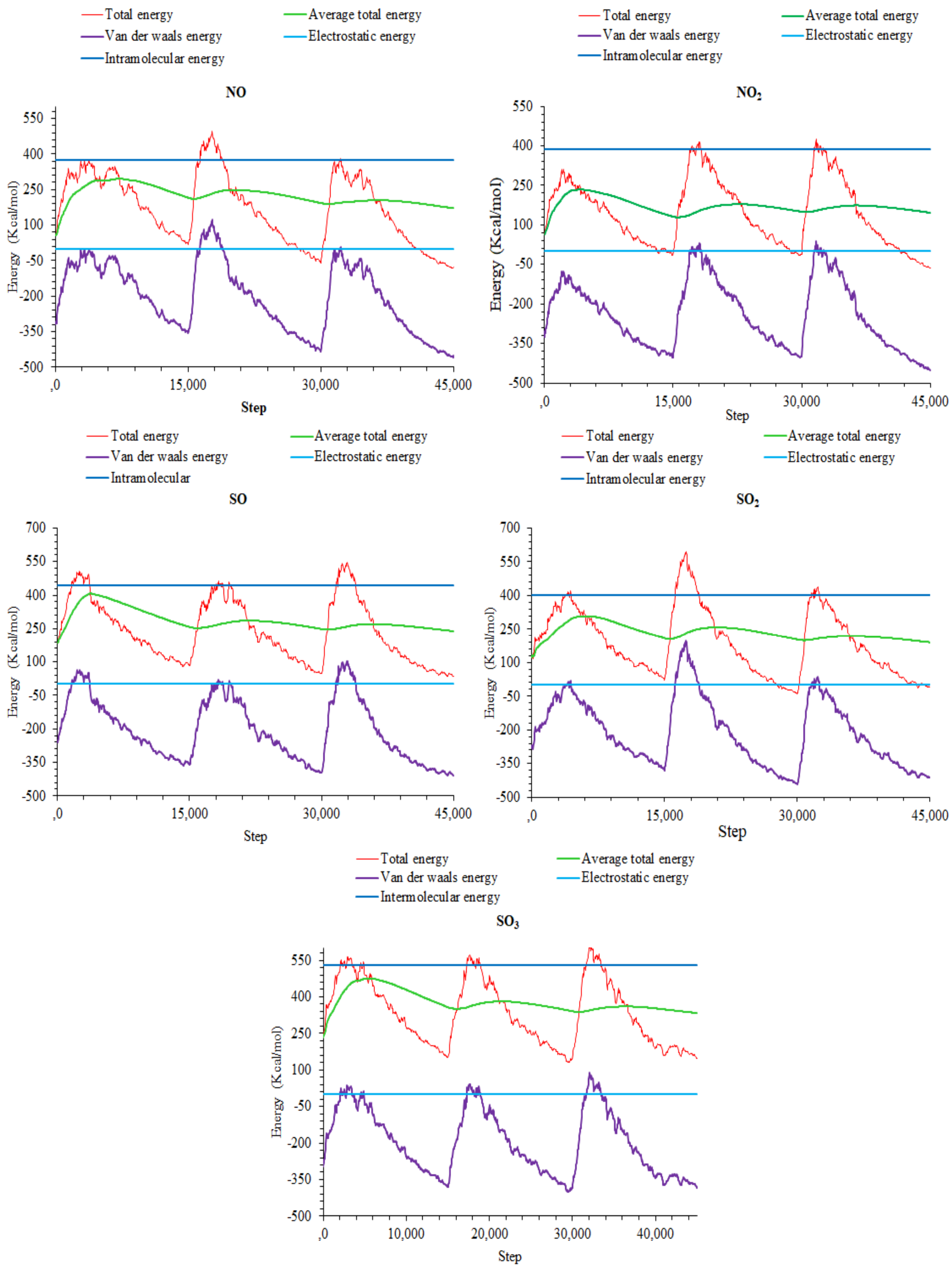

Figure 3. Total energy distributions for the GM/500H_2O/$NaMgPO_4$(033) system.

Figure 4 shows the lateral views of the least energy adsorption model for single gaseous molecules, including NO, NO_2, SO, SO_2, and SO_3, on the surface of $NaMgPO_4$ (033) in an aqueous medium. On the other hand, the NO, NO_2, and SO_2 molecules are oriented in parallel on the surface of $NaMgPO_4$, while the other molecules SO_3 and SO adsorb horizontally. The side views of the most stable adsorption configurations for all chemical complexes demonstrate that there is an interaction between the sorbates and the sorbent that involves electron donation and acceptance. To reinforce the ratio, all of the molecules adsorb at different distances on the adsorbent's surface.

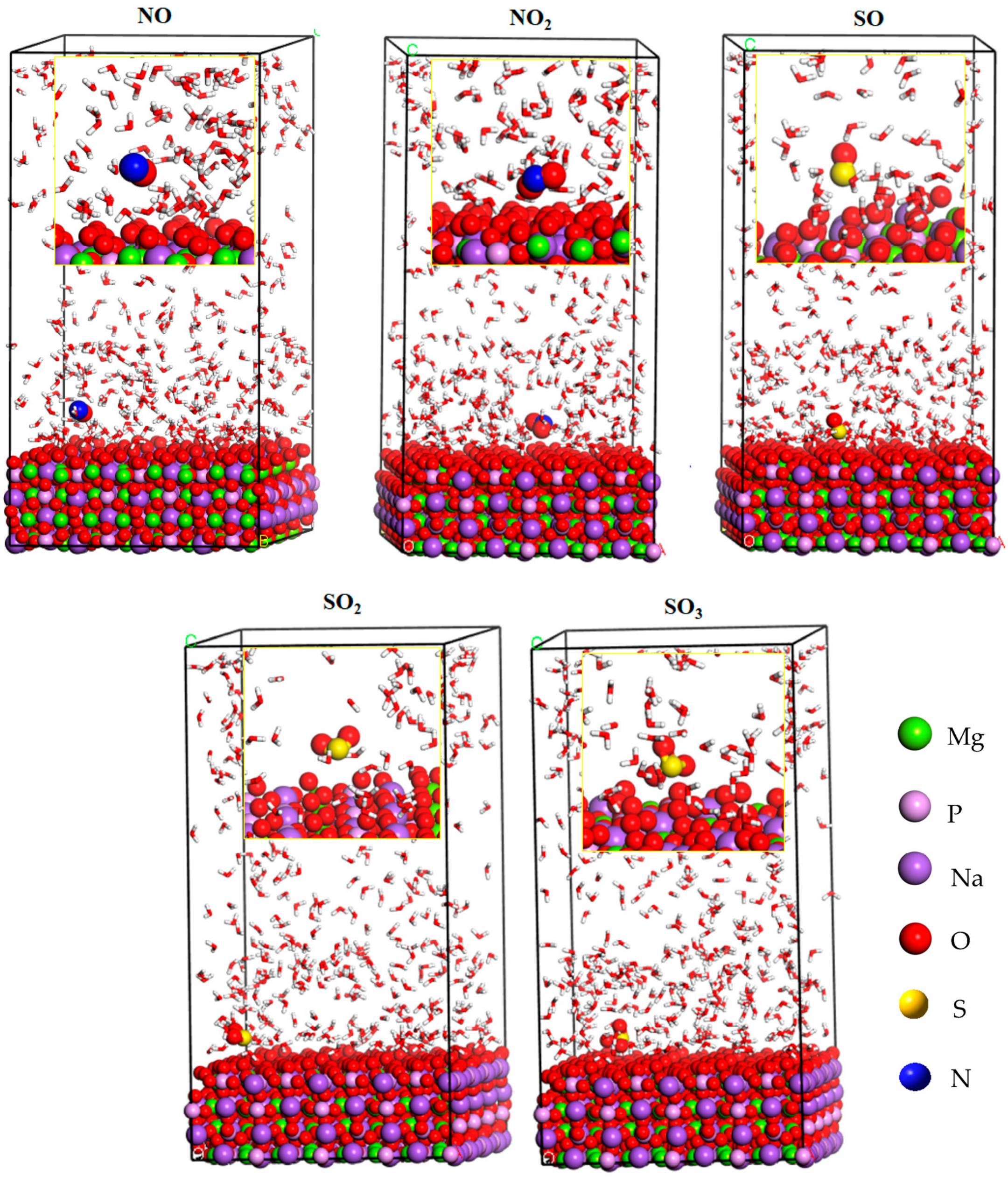

Figure 4. Equilibrium configurations for the GM/500H_2O/$NaMgPO_4$ (033) system.

The evaluation of outputs for energies determined by the MCDS are summarized in Table 4, including the total (E_{Tot}), adsorption (E_{ads}), rigid adsorption (RAE), and deformation (E_{def}) energies. Thus, Eads is the energy required to adsorb a substance onto a solid surface. Then, the RAE is the energy required to adsorb a substance onto a surface without allowing for any deformation of the adsorbate or the surface. Therefore, the Edef is the energy required to deform the adsorbate or the surface during the adsorption process. The relaxation of adsorbates on the surface refers to the way in which the adsorbates rearrange themselves on the surface in order to minimize their total energy. Furthermore, the relaxation of the adsorbates on the $NaMgPO_4$ surface (033) is due to a low strain energy, and (d_{Eads}/dN_i) is the differential adsorption energy required to detach or remove a single molecule from the studied adsorbent surface.

Table 4. Monte Carlo simulation outputs of the GMs on $NaMgPO_4$ (kcal/mol).

Molecule	E_{total}	E_{ads}	RAE	E_{def}	dE_{ads}/dNi_{H2O}	dE_{ads}/dN_i
NO	−472.031	−874.033	−472.563	−374.469	−0.764	−2.218
NO_2	−433.835	−819.943	−434.982	−384.961	−0.781	−13.714
SO	−481.969	−924.810	−482.146	−442.664	−0.766	−72.933
SO_2	−474.448	−876.333	−475.027	−401.306	−0.769	−31.010
SO_3	−447.572	−977.714	−453.463	−524.251	−0.804	−155.016

The outcomes demonstrate that all adsorption energy values were generally negative, with the GM-$NaMgPO_4$ complexes often having a greater absolute value. As shown in Table 4, the GMs are firmly adsorbed onto the $NaMgPO_4$ (033) surface due to the higher negative values of adsorption energy. Obviously, the values obtained show that the SO_3-$NaMgPO_4$ complex has the highest negative adsorption energy of all studied gaseous molecules, calculated at −977.714 kcal/mol, which means that the SO_3 molecule is more adsorbed onto the $NaMgPO_4$ (033) surface than the other NO, NO_2, SO, and SO_2 molecules (−874.033, −819.943, −924.81, and −876.333 in kcal/mol, respectively). As a result, the adsorption energy and relative stability of all complexes are as follows: SO_3/500 H_2O/$NaMgPO_4$ (033), SO/500 H_2O/$NaMgPO_4$ (033), SO_2/500 H_2O/$NaMgPO_4$ (033), NO/500 H_2O/$NaMgPO_4$ (033), and NO_2/500 H_2O/$NaMgPO_4$ (033). Thus, their negative E_{ads} values characterize all systems with the strongest and most spontaneous adsorption [50]. The high absolute Eads values for all complexes GM-$NaMgPO_4$ indicate that all gaseous molecules in an aqueous solution are significantly adsorbed onto the $NaMgPO_4$ (033) face, possibly via a chemical bond. As shown in Table 4, all adsorption, deformation energies, dE_{ads}/dNi_{MG}, and $dEads/dNi_{H2O}$ values obtained for SO_3 are higher than those obtained for the NO, NO_2, SO, and SO_2 molecules. This study demonstrates that, in an aqueous medium, SO3 may have chemical characteristics that make it stable and interact strongly with the $NaMgPO_4$ surface. The returning absolute dE_{ads}/dNi value for the SO_3 molecule (−155.016 kcal/mol) is higher than that of the NO, NO_2, SO, and SO_2 molecules (−2.218, −13.714, −72.933, and −31.010 kcal/mol, respectively), which reveals that SO_3 adsorption occurs with ease on the $NaMgPO_4$ surface in aqueous media. The higher absolute dE_{ads}/dNi_{H2O} value for the SO_3 molecule (−0.804 kcal/mol), compared with those of the NO, NO_2, SO, and SO_2 molecules (−0.764, −0.781, −0.766, and −0.769 kcal/mol, respectively), suggests that the SO_3 molecule is more strongly adsorbed onto the solid surface and that it forms more hydrogen bonds with the solid surface.

3.6. Radial Distribution Function

The radial distribution function (RDF) is important to define the physisorption or chemi-sorption process that takes place on the adsorbent surface during adsorption [51]. Furthermore, the specific distance at which the peaks occur can also provide additional information about the nature of the interaction between the adsorbate and the adsorbent. In general, the chemisorption process is typically simplified when the peaks are present between 1 and 3.5 Å, while the appearance of peaks at distances greater than 3.5 Å suggests as an indication of the physisorption process. The RDF peak values of the oxygen, sulfur, and nitrogen atoms for NO, NO_2, SO, SO_2, and SO_3 and the $NaMgPO_4$ (033) interface are shown in Figure 5.

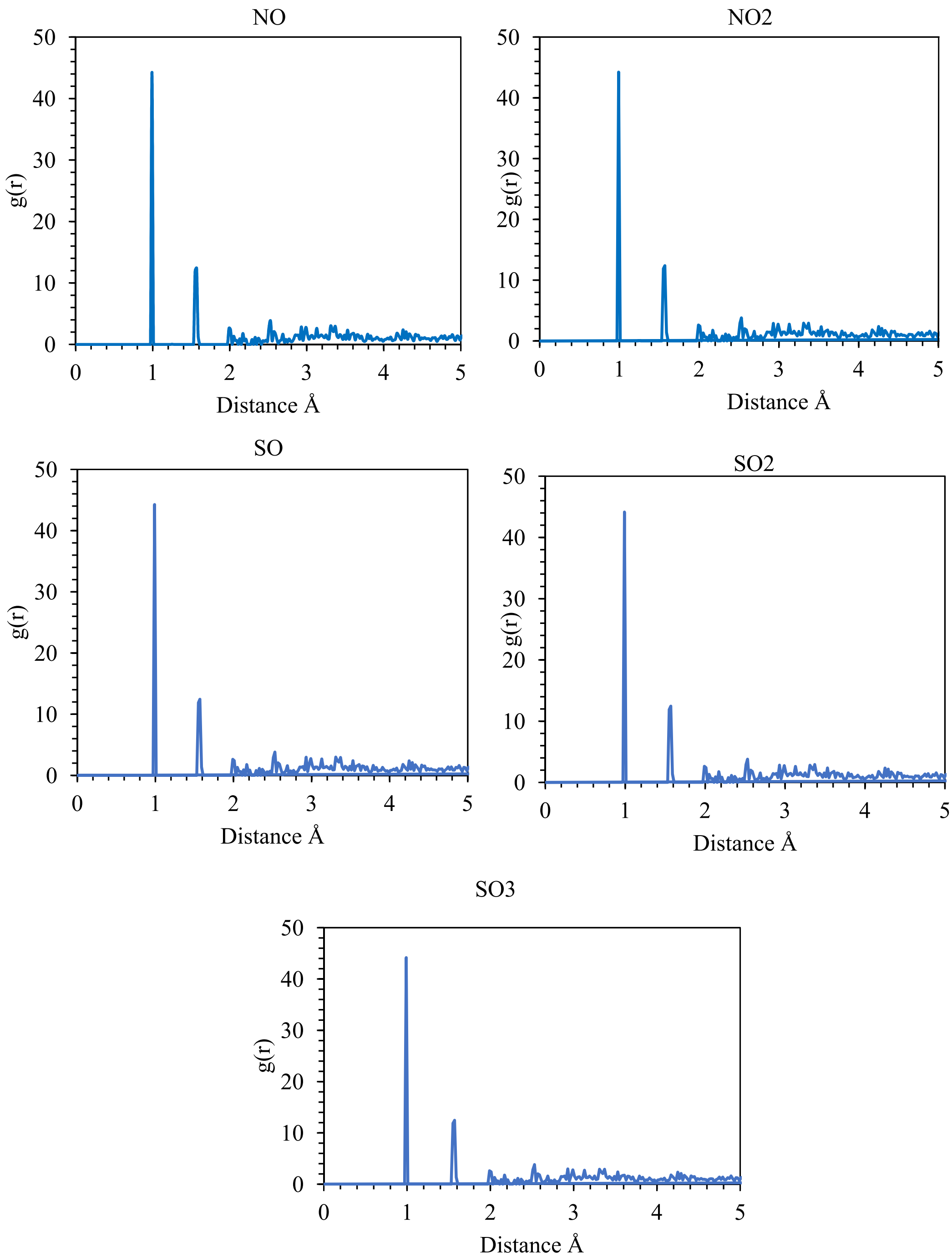

Figure 5. Intermolecular interaction of the GM/$NaMgPO_4$ (033) system.

As shown in Figure 5, a strong bond was formed between the chemisorbed GMs and the $NaMgPO_4$ face, as evidenced by the fact that all the lowest link distances between the GMs and $NaMgPO_4$ (033) face were less than 3.5 Å. Moreover, the NO, NO_2, SO, SO_2, and SO_3 molecules appear to interact strongly with the surface of $NaMgPO_4$ (033). These data indicate that the GMs are firmly adsorbed on the $NaMgPO_4$ surface in an aqueous phase via covalent bonding. The GMs and $NaMgPO_4$ displayed the lowest bond distances of 0.99, 1.55, and 1.59 Å. These distance values suggest that a chemical link (within the chemisorption region) was formed between the GMs and the surface of $NaMgPO_4$ (033). In this study, a variety of nucleophilic and electrophilic attack centers (especially heteroatoms) were used to theoretically show that both chemical compounds under investigation are virtually parallel to the adsorbent face. Additionally, the heteroatoms lead to an electron exchange with the open orbitals of the adsorbent [52]. This caused a connection to form between the chosen molecules and $NaMgPO_4$. When certain gaseous molecules come into contact with an adsorbent, they adhere to the substrate to form an adsorbed layer. This material is typically referred to as an adsorbent or substrate, whereas the resultant of the adsorbed molecules is named adsorbate. We can distinguish between physisorption and chemisorption due to the natural forces at play. The excess electrons on the substrate can be transferred from it to the active sites of the investigated molecules (back-donation) [52].

4. Conclusions

In the present study, the adsorption behavior of the NO, NO_2, SO, SO_2, and SO_3 gaseous molecules on the $NaMgPO_4$ adsorbent was predicted using density functional theory at B3LYP with a LANL2DZ basis and Monte Carlo dynamic simulation. The reactivity indices, frontier molecular orbitals (FMO), and MEP maps were performed. The analysis of the calculated HOMO and LUMO energies revealed the evident charge transfer within the molecules. The MEP graph indicated that electrophilic sites were mostly found near oxygen atoms, while nucleophilic sites were located near nitrogen atoms and sulfur atoms. This shows that gaseous molecules can interact with the adsorbent surface through an electron donor–acceptor reaction. The Monte Carlo dynamic simulation indicated that all GM-$NaMgPO_4$ (with GMs = NO, NO_2, SO, SO_2, and SO_3) complexes in an aqueous medium exhibited a negative adsorption energy, with values of −819.943, −874.033, −876.333, −924.810, and −977.714 kcal/mol, respectively. These negative E_{ads} values indicate that GM adsorption is strong and spontaneous. Also, the MCD simulation suggested that the SO, NO, and SO_3 molecules were adsorbed in a parallel manner on the $NaMgPO_4$ surface, while the SO_2 and NO_2 molecules were adsorbed horizontally. Furthermore, due to the high absolute E_{ads} value, the GM adsorption on the $NaMgPO_4$ (033) surface was of the chemical type and suggests that a strong interaction took place. These results were confirmed by RDF analyses. Moreover, the SO_3-$NaMgPO_4$ complex had a higher $\Delta E_{ads}/dNi$, with a value of −155.016 kcal/mol, compared to the other complexes, indicating that SO_3 is more adsorbed on the $NaMgPO_4$ (033) surface.

Author Contributions: Conceptualization, J.A., M.K., A.M. and M.A. (Mohamed Abdennouri); methodology, M.A. (Mohamed Abdennouri); software, J.A., M.K. and A.M.; validation, N.B., and M.A. (Mohamed Abdennouri); formal analysis, W.B., H.H., M.S. and M.A. (Mounia Achak); investigation, J.A.; data curation, A.M., M.S. and N.B.; writing—original draft preparation, J.A.; writing—review and editing, M.K., W.B., H.H., M.A. (Mounia Achak), N.B. and M.A. (Mohamed Abdennouri); supervision, M.A. (Mohamed Abdennouri); project administration, M.A. (Mohamed Abdennouri). All authors have read and agreed to the published version of the manuscript.

Funding: This research received no specific grant from any funding agency in the public, commercial, or not-for-profit sectors.

Institutional Review Board Statement: Not applicable.

Informed Consent Statement: Not applicable.

Data Availability Statement: The datasets used and/or analyzed during this study are available from the corresponding author on reasonable request.

Conflicts of Interest: The authors declare no conflict of interest.

References

1. Zhu, L.; Zhong, Z.; Yang, H.; Wang, C.; Wang, L. DeNOx performance and characteristic study for transition metals doped iron-based catalysts. *Korean J. Chem. Eng.* **2017**, *34*, 1229. [CrossRef]
2. Shahzad, K.; Saleem, M.; Ghauri, M.; Akhtar, J.; Ali, N.; Akhtar, N.A. Combustion Science and 6th Asian Physics Symposium. *IOP Publ. J. Phy. Conf. Ser.* **2015**, *187*, 1079–1092.
3. Nugraha; Saputro, A.G.; Agusta, M.K.; Yuliarto, B.; Dipojono, H.K.; Maezono, R. Density functional study of adsorptions of CO_2, NO_2 and SO_2 molecules on Zn(0002) surfaces. *J. Phys. Conf. Ser.* **2016**, *739*, 012080. [CrossRef]
4. Streets, D.; Waldhoff, S. Present and future emissions of air pollutants in China: SO_2, NOx, and CO. *Atmos. Environ.* **2000**, *34*, 363–374. [CrossRef]

5. Sakai, Y.; Koyanagi, M.; Mogi, K.; Miyoshi, E. Theoretical study of adsorption of SO_2 on Ni(111) and Cu(111) surfaces. *Surf. Sci.* **2002**, *513*, 272–282. [CrossRef]
6. Lin, F.; Wu, X.; Liu, S.; Weng, D.; Huang, Y. Preparation of MnO_x-CeO_2–Al_2O_3 mixed oxides for NO_x-assisted soot oxidation: Activity, structure and thermal stability. *J. Chem. Eng.* **2013**, *226*, 105–112. [CrossRef]
7. Zhang, Y.; Yu, Y.B.; He, H. Oxygen vacancies on nanosized ceria govern the NO_x storage capacity of NSR catalysts. *Catal. Sci. Technol.* **2016**, *6*, 3950–3962. [CrossRef]
8. Rezaei, F.; Rownaghi, A.A.; Monjezi, S.; Lively, R.P.; Jones, C.W. SO_x/NO_x removal from flue gas streams by solid adsorbents: A review of current challenges and future directions. *Energy Fuels* **2015**, *29*, 5467–5486. [CrossRef]
9. Liu, L.; Gao, X.; Song, H.; Zheng, C.H.; Zhu, X.B.; Luo, Z.Y.; Ni, M.J.; Cen, K.F. Study of the promotion effect of iron on supported manganese catalysts for NO oxidation. *Aerosol. Air Qual. Res.* **2014**, *14*, 1038–1046. [CrossRef]
10. Guo, R.T.; Chen, Q.L.; Ding, H.L.; Wang, Q.S.; Pan, W.G.; Yang, N.Z.; Lu, C.Z. Preparation and characterization of CeO_x@MnO_x core-shell structure catalyst for catalytic oxidation of NO. *Catal. Commun.* **2015**, *69*, 165–169. [CrossRef]
11. Zahaf, R.; Jung, J.W.; Coker, Z.; Kim, S.; Choi, T.Y.; Lee, D. Pt catalyst over SiO_2 and Al_2O_3 supports synthesized by aerosol method for HC-SCR $DeNO_x$ application. *Aerosol. Air Qual. Res.* **2015**, *15*, 2409–2421. [CrossRef]
12. Chen, T.; Lin, H.; Guan, B.; Gong, X.; Li, K.; Huang, Z. Promoting the low temperature activity of Ti–V–O catalysts by premixed flame synthesis. *J. Chem. Eng.* **2016**, *296*, 45–55. [CrossRef]
13. Guo, R.T.; Sun, P.; Pan, W.G.; Li, M.Y.; Liu, S.M.; Sun, X.; Liu, S.W.; Liu, J. A highly effective $MnNdO_x$ catalyst for the selective catalytic reduction of NO_x with NH_3. *Ind. Eng. Chem. Res.* **2017**, *56*, 12566–12577. [CrossRef]
14. Granger, P.; Parvulescu, V.I. Catalytic NO_x Abatement Systems for Mobile Sources: From Three-Way to Lean Burn after-Treatment Technologies. *Chem. Rev.* **2011**, *111*, 3155–3207. [CrossRef]
15. Feng, H.; Wang, C.; Huang, Y. Particle deposition behaviors of monolithic De-NO_x catalysts for selective catalytic reduction (SCR). *Korean J. Chem. Eng.* **2017**, *34*, 2832–2839. [CrossRef]
16. Jackson, G.J.; Driver, S.M.; Woodruff, D.P.; Abrams, N.; Jones, R.G.; Butterfield, M.T.; Rapper, M.D.C.; Cowied, B.C.C.; Formoso, V. A structural study of the interaction of SO_2 with Cu(111). *Surf. Sci.* **2000**, *459*, 231–244. [CrossRef]
17. Terada, S.; Yokoyama, T.; Sakano, M.; Kiguchi, M.; Kitajima, Y.; Ohta, T. Asymmetric surface structure of SO_2 on Pd(111) studied by total-reflection X-ray absorption fine structure spectroscopy. *Chem. Phys. Lett.* **1999**, *300*, 645–650. [CrossRef]
18. Wilson, K.; Hardacre, C.; Baddeley, C.J.; Ludecke, J.; Woodruff, D.P.; Lsmbert, R.M. A spectroscopic study of the chemistry and reactivity of SO_2 on Pt{111}: Reactions with O_2, CO and C_3H_6. *Surf. Sci.* **1997**, *372*, 279–288. [CrossRef]
19. Harrison, M.J.; Woodruff, D.P.; Robinson, J. Density functional theory investigation of the structure of SO_2 and SO_3 on Cu(111) and Ni(111). *Surf. Sci.* **2006**, *600*, 1827–1836. [CrossRef]
20. Wanglai, C.; Meiling, H.; Jie, L.; Shandong, Y.; Yongjun, L.; Yinghao, C. Oxidation of SO_2 and NO by epoxy groups on graphene oxides: The role of the hydroxyl group. *RSC Adv.* **2015**, *5*, 22802–22810.
21. Oladele, E.O.; Alabi, A.H.; Olawale, M.D.; Ishaya, F.A. Adsorption of methylene blue dye from stimulated wastewater onto modified and unmodified cassis fistula pods: Kinetics, thermodynamics and equilibrium studies. *UNIOSUN J. Sci.* **2019**, *4*, 1–14.
22. Monticelli, O.; Loenders, R.; Jacobs, P.A.; Martens, J.A. NO_x removal from exhaust gas from lean burn internal combustion engines through adsorption on FAU type zeolites cation exchanged with alkali metals and alkaline earth metals. *Appl. Catal. B Environ.* **1999**, *21*, 215–220. [CrossRef]
23. Li, L.; Chen, J.; Zhang, S.; Guan, N.; Wang, T.; Liu, S. Selective catalytic reduction of nitrogen oxides from exhaust of lean burn engine over in situ synthesized monolithic Cu–TS-1/cordierite. *Catal. Today* **2004**, *90*, 207–213. [CrossRef]
24. Sultana, A.; Habermacher, D.D.; Kirschhock, C.E.A.; Martens, J.A. Adsorptive separation of NO_x in presence of SO_x from gas mixtures simulating lean burn engine exhaust by pressure swing process on Na-Y zeolite. *Appl. Catal. B Environ.* **2004**, *48*, 65–76. [CrossRef]
25. Barka, N.; Assabbane, A.; Nounahb, A.; Laanab, L.; Ichou, Y.A. Removal of textile dyes from aqueous solutions by natural phosphate as a new adsorbent. *Desalination* **2009**, *235*, 264–275. [CrossRef]
26. Sajid, H.; Siddique, S.A.; Ahmed, E.; Arshad, M.; Gilani, M.A.; Rauf, A.; Imran, M.; Mahmood, T. DFT outcome for comparative analysis of $Be_{12}O_{12}$, $Mg_{12}O_{12}$ and $Ca_{12}O_{12}$ nanocages toward sensing of N_2O, NO_2, NO, H_2S, SO_2 and SO_3 gases. *Comput. Theor. Chem.* **2022**, *1211*, 113694. [CrossRef]
27. Gao, Z.; Li, L.; Huang, H.; Xu, S.; Yan, G.; Zhao, M.; Ding, Z. Adsorption characteristics of acid gases (NO, NO_2, SO_2 and SO_3) on different single-atom nickel adsorbent: A first-principles study. *Appl. Surf. Sci.* **2020**, *527*, 146939. [CrossRef]
28. Siddique, S.A.; Sajid, H.; Gilani, M.A.; Ahmed, E.; Arshad, M.; Mahmood, T. Sensing of SO_3, SO_2, H_2S, NO_2 and N_2O toxic gases through aza-macrocycle via DFT calculations. *Comput. Theor. Chem.* **2022**, *1209*, 113606. [CrossRef]
29. Balakrishna, A.; Ntwaeaborwa, O.M. Study of luminescent behavior and crystal defects of different MNa[PO_4]-Dy^{3+} phosphors (M = Mg, Ca, Sr and Ba). *Sens. Actuators B Chem.* **2017**, *242*, 305–317. [CrossRef]
30. Bhavya, N.R.; Mahendra, M.; Doreswamy, B.H.; Kumar, S.; Gilandoust, M.; El-khatatneh, N.A. Computational and spectroscopic investigations on boronic acid based fluorescent carbohydrate sensor in aqueous solution at physiological pH 7. *5. J. Mol. Struct.* **2019**, *1194*, 305–319. [CrossRef]
31. Hay, P.J.; Wadt, W.R. Ab initio effective core potentials for molecular calculations. Potentials for the transition metal atoms Sc to Hg. *J. Chem. Phys.* **1985**, *82*, 270–283. [CrossRef]

32. Shokuhi Rad, A.; Zardoost, M.R.; Abedini, E. First-principles study of terpyrrole as a potential hydrogen cyanide sensor: DFT calculations. *J. Mol. Model.* **2015**, *21*, 273. [CrossRef] [PubMed]
33. Pearson, R.G. Absolute electronegativity and hardness: Application to inorganic chemistry. *Inorg. Chem.* **1988**, *27*, 734–740. [CrossRef]
34. Pearson, R.G. Chemical hardness and density functional theory. *J. Chem. Sci.* **2005**, *117*, 369–377. [CrossRef]
35. Geerling, P.; Prof, F.D.; Langenaeker, W. Conceptual density functional theory. *Chem. Rev.* **2003**, *103*, 1793–1874. [CrossRef] [PubMed]
36. Pearson, R.G.; Szentpaly, L.; Liu, S. Electrophilicity index. *J. Am. Chem. Soc.* **1999**, *121*, 1922–1924.
37. Kaya, S.; Guo, L.; Kaya, C.; Tüzün, B.; Obot, I.B.; Touir, R.; Islam, N. Quantum chemical and molecular dynamic simulation studies for the prediction of inhibition efeciencies of some piperidine derivatives on the corrosion of iron, J. *Taiwan Inst. Chem. Eng.* **2016**, *65*, 522–529. [CrossRef]
38. *BIOVIA Materials Studio Version 8.0*; Accelrys Inc.: San Diego, CA, USA, 2016.
39. Khnifira, M.; El Hamidi, S.; Sadiq, M.; Şimşek, S.; Kaya, S.; Barka, N.; Abdennouri, M. Adsorption mechanisms investigation of methylene blue on the (001) zeolite 4A surface in aqueous medium by computational approach and molecular dynamics. *Appl. Surf. Sci.* **2022**, *572*, 151381. [CrossRef]
40. Hsissou, R.; Benhiba, F.; Abbout, S.; Dagdag, O.; Benkhaya, S.; Berisha, A.; Erramli, H.; Elharfi, A. Trifunctional epoxy polymer as corrosion inhibition material for carbon steel in 1.0 M HCl: MD simulations, DFT and complexation computations. *Inorg. Chem. Commun.* **2020**, *115*, 107858. [CrossRef]
41. Ajebli, S.; Kaichouh, G.; Khachani, M.; Babas, H.; El Karbane, M.; Warad, I.; Safi, Z.S.; Berisha, A.; Mehmeti, V.; Guenbour, A.; et al. The adsorption of Tenofovir in aqueous solution on activated carbon produced from maize cobs: Insights from experimental, molecular dynamics simulation, and DFT calculations. *Chem. Phys. Lett.* **2022**, *801*, 139676. [CrossRef]
42. Khnifira, M.; El Hamidi, S.; Machrouhi, A.; Mahsoune, A.; Boumya, W.; Tounsadi, H.; Mahjoubi, F.Z.; Sadiq, M.; Barka, N.; Abdennouri, M. Theoretical and experimental study of the adsorption characteristics of Methylene Blue on titanium dioxide surface using DFT and Monte Carlo dynamic simulation. *Desalin. Water Treat.* **2020**, *190*, 393–411. [CrossRef]
43. Kokalj, A. Molecular modeling of organic corrosion inhibitors: Calculations, pitfalls, and conceptualization of molecule–surface bonding. *Corros. Sci.* **2021**, *193*, 109650. [CrossRef]
44. Vengatesh, G.; Sundaravadivelu, M. Experimental and theoretical evaluation of new piperidine and oxaquinuclidine core containing derivatives as an efficient corrosion inhibitor for copper in nitric acid medium. *J. Adhes. Sci. Technol.* **2020**, *34*, 2075–2106. [CrossRef]
45. Wang, H.; Wang, X.; Wang, H.; Wang, L.; Liu, A. DFT study of new bipyrazole derivatives and their potential activity as corrosion inhibitors. *J. Mol. Model.* **2007**, *13*, 147–153. [CrossRef] [PubMed]
46. Sastri, V.S.; Perumareddi, J.R. Molecular Orbital Theoretical Studies of Some Organic Corrosion Inhibitors. *Corros. Sci.* **1997**, *53*, 617–622. [CrossRef]
47. Abdulazeez, M.O.; Oyebamiji, A.K.; Semire, B. DFT and QSAR study of corrosion inhibition on 3,5-di-substituted pyrazol derivatives with heteroatom on position one. *Leban. Sci. J.* **2016**, *17*, 217–232. [CrossRef]
48. Zhao, H.; Yang, Y.; Shu, X.; Wang, Y.; Ran, Q. Adsorption of organic molecules on mineral surfaces studied by first-principle calculations: A review. *Adv. Colloid Interface Sci.* **2018**, *256*, 230–241. [CrossRef]
49. Khnifira, M.; Mahsoune, A.; Belghiti, M.E.; Khamar, L.; Sadiq, M.; Abdennouri, M.; Barka, N. Combined DFT and MD simulation approach for the study of SO_2 and CO_2 adsorption on graphite (111) surface in aqueous medium. *CRGSC Curr. Res. Green Sustain. Chem.* **2021**, *4*, 100085. [CrossRef]
50. Kondori, J.; Zendehboudi, S.; James, L. Molecular dynamic simulations to evaluate dissociation of hydrate structure II in the presence of inhibitors: A mechanistic study, Chem. *Eng. Res. Des.* **2019**, *149*, 81–94. [CrossRef]
51. Khnifira, M.; Boumya, W.; Attarki, J.; Mahsoune, A.; Abdennouri, M.; Sadiq, M.; Kaya, S.; Barka, N. Elucidating the adsorption mechanisms of anionic dyes on chitosan (110) surface in aqueous medium by quantum chemical and molecular dynamics. *Mater. Today Commun.* **2022**, *33*, 104488. [CrossRef]
52. Khnifira, M.; Boumya, W.; Attarki, J.; Soufi, A.; Sadiq, M.; Achak, M.; Barka, N.; Abdennouri, M. Interaction between drug molecule and inverse spinel surfaces in aqueous solution: Insights from DFT and DMC simulation. *Comput. Theor. Chem.* **2023**, *1228*, 114289. [CrossRef]